# Dirac cones reshaped by interaction effects in suspended graphene

D. C. Elias[1], R. V. Gorbachev[1], A. S. Mayorov[1], S. V. Morozov[2], A. A. Zhukov[3], P. Blake[3], L. A. Ponomarenko[1], I. V. Grigorieva[1], K. S. Novoselov[1], F. Guinea[4]★ and A. K. Geim[1,3]

In graphene, electron–electron interactions are expected to play a significant role, as the screening length diverges at the charge neutrality point and the conventional Landau theory that enables us to map a strongly interacting electronic liquid into a gas of non-interacting fermions is no longer applicable[1,2]. This should result in considerable changes in graphene's linear spectrum, and even more dramatic scenarios, including the opening of an energy gap, have also been proposed[3-5]. Experimental evidence for such spectral changes is scarce, such that the strongest is probably a 20% difference between the Fermi velocities v_F found in graphene and carbon nanotubes[6]. Here we report measurements of the cyclotron mass in suspended graphene for carrier concentrations n varying over three orders of magnitude. In contrast to the single-particle picture, the real spectrum of graphene is profoundly nonlinear near the neutrality point, and v_F describing its slope increases by a factor of more than two and can reach $\approx 3 \times 10^6\,\mathrm{m\,s^{-1}}$ at $n < 10^{10}\,\mathrm{cm^{-2}}$. No gap is found at energies even as close to the Dirac point as $\sim 0.1\,\mathrm{meV}$. The observed spectral changes are well described by the renormalization group approach, which yields corrections logarithmic in n.

In the first approximation, charge carriers in graphene behave like massless relativistic particles with a conical energy spectrum $E = v_F \hbar k$ where the Fermi velocity v_F plays the role of the effective speed of light and k is the wave vector. Because graphene's spectrum is filled with electronic states up to the Fermi energy, their Coulomb interaction has to be taken into account. To do this, the standard approach of Landau's Fermi-liquid theory, proven successful for normal metals, fails in graphene, especially at E close to the neutrality point, where the density of states vanishes. This leads to theoretical divergences that have the same origin as those in quantum electrodynamics and other interacting-field theories. In the latter case, the interactions are normally accounted for by using the renormalization group theory[1], that is, by defining effective models with a reduced number of degrees of freedom and treating the effect of high-energy excitations perturbatively. This approach was also applied to graphene by using as a small parameter either the effective coupling constant $\alpha = e^2/\hbar v_F$ (refs 7,8) or the inverse of the number of fermion species in graphene $N_f = 4$ (refs 9,10). The resulting many-body spectrum is shown in Fig. 1.

As for experiment, graphene placed on top of an oxidized Si wafer and with typical $n \approx 10^{12}\,\mathrm{cm^{-2}}$ exhibits v_F with the conventional value $v_F^* \approx 1.05 \pm 0.1 \times 10^6\,\mathrm{m\,s^{-1}}$. The value was measured by using a variety of techniques including the early transport experiments, in which Shubnikov–de Haas oscillations (SdHO) were analysed to extract v_F (refs 11,12). It has been noted
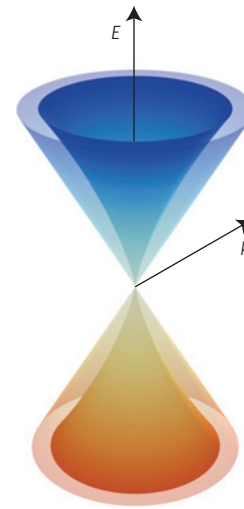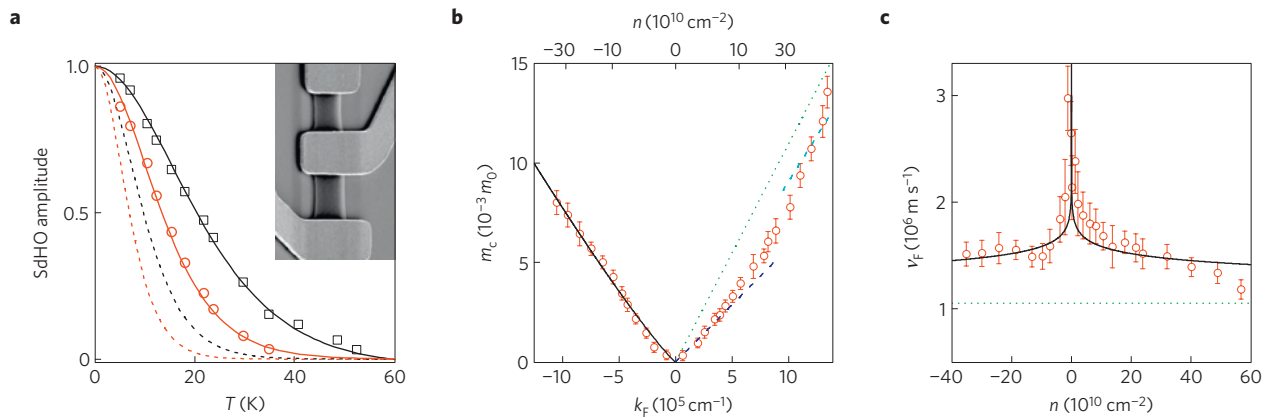

Figure 1 | Sketch of graphene's electronic spectrum with and without taking into account e–e interactions. The outer cone is the single-particle spectrum $E = v_F \hbar k$, and the inner cone illustrates the many-body spectrum predicted by the renormalization group theory and observed in the current experiments. We need to consider this image as follows. Electron–electron (e–e) interactions reduce the density of states at low E and lead to an increase in v_F that slowly (logarithmically) diverges at zero E. As the Fermi energy changes, v_F changes accordingly but remains constant under the Fermi surface (note the principal difference from the excitation spectra that probe the states underneath the surface[28]).

that v_F^* is larger than $v_F^0 \approx 0.85 \pm 0.05 \times 10^6\,\mathrm{m\,s^{-1}}$, where v_F^0 is the value accepted for metallic carbon nanotubes (see, for example, ref. 6). In agreement with this notion, the energy gaps measured in semiconducting nanotubes show a nonlinear dependence on their inverse radii, which is consistent with the larger v_F in flat graphene[6]. The differences between v_F in graphene and its rolled-up version can be attributed to e–e interactions[13]. Another piece of evidence came from infrared measurements[14] of the Pauli blocking in graphene, which showed a sharp (15%) decrease in v_F on increasing n from ≈ 0.5 to $2 \times 10^{12}\,\mathrm{cm^{-2}}$. A similar increase in v_F ($\approx 25\%$) for similar n has recently been found by scanning tunnelling spectroscopy[15]. In both cases, the changes were sharper and larger than the theory predicts for the probed relatively small intervals of n.

Here, we have studied SdHO in suspended graphene devices (inset in Fig. 2a). They were fabricated by using the procedures

[1]School of Physics & Astronomy, University of Manchester, Manchester M13 9PL, UK, [2]Institute for Microelectronics Technology, 142432 Chernogolovka, Russia, [3]Manchester Centre for Mesoscience & Nanotechnology, University of Manchester, Manchester M13 9PL, UK, [4]Instituto de Ciencia de Materiales de Madrid (CSIC), Sor Juana Inés de la Cruz 3, Madrid 28049, Spain. *e-mail: paco.guinea@icmm.csic.es.

Figure 2 | Probing graphene's electronic spectrum through SdHO. a, Symbols show examples of the T dependence of SdHO for $n \approx +1.4$ and -7.0×10^{10} cm^{-2} for electrons and holes, respectively. The dependence is well described by the Lifshitz–Kosevich formula (solid curves). The dashed curves are the behaviour expected for $v_F = v_F^*$ (in the matching colours). The inset shows a scanning electron micrograph of one of our devices. The vertical graphene wire is $\approx 2\,\mu$m wide and suspended above an oxidized Si wafer attached to Au/Cr contacts. Approximately half of the 300-nm-thick SiO$_2$ was etched away underneath the graphene structure. **b,** m_c as a function of k_F for the same device. m_0 is the free-electron mass. It is the exponential dependence of the SdHO amplitude on m_c that enables high accuracy of the cyclotron-mass measurements. The error bars indicate maximum and minimum values of m_c that could fit data such as in **a**. The dashed curves are the best linear fits $m_c \propto n^{1/2}$ at high and low n. The dotted line is for the standard value of $v_F = v_F^*$. Graphene's spectrum renormalized owing to e–e interactions is expected to result in the dependence shown by the solid curve. **c,** m_c re-plotted in terms of varying v_F. The colour scheme is to match the corresponding data in **b**.

described previously[16–18]. After current annealing, our devices exhibited record mobilities $\mu \sim 1{,}000{,}000$ cm^2 Vs^{-1}, and charge homogeneity δn was better than 10^9 cm^{-2} such that we observed the onset of SdHO in magnetic fields $B \approx 0.01$ T and the first quantum Hall plateau became clearly visible in B below 0.1 T (see Supplementary Information). To extract the information about graphene's electronic spectrum, we employed the following routine. SdHO were measured at various B and n as a function of temperature (T). Their amplitude was then analysed by using the standard Lifshitz–Kosevich formula $T/\sinh(2\pi^2 T m_c/\hbar e B)$, which holds for the Dirac spectrum[19] and enables us to find the effective cyclotron mass m_c at a given n. This approach was previously employed for graphene on SiO$_2$, and it was shown that, within experimental accuracy and for a range of $n \sim 10^{12}$ cm^{-2}, m_c was well described by dependence $m_c = \hbar(\pi n)^{1/2}/v_F^*$, which corresponds to the linear spectrum[11,12]. With respect to the earlier experiments, our suspended devices offer critical advantages. First, in the absence of a substrate, interaction-induced spectral changes are expected to be maximal because no dielectric screening is present. Second, the high quality of suspended graphene has enabled us to probe its spectrum over a very wide range of n, which is essential as the spectral changes are expected to be logarithmic in n. Third, owing to low δn, we can approach the Dirac point within a few millielectronvolts. This low-E regime, in which a major renormalization of the Dirac spectrum is expected, has previously been inaccessible.

Figure 2a shows examples of the T dependence of the SdHO amplitude at low n (for details, see Supplementary Information). The curves are well described by the Lifshitz–Kosevich formula but the inferred m_c are half those expected if we assume that v_F retains its conventional value v_F^*. To emphasize this profound discrepancy with the earlier experiments, the dashed curves in Fig. 2a plot the T dependence expected under the assumption $v_F = v_F^*$. The SdHO would then have to decay twice as fast with increasing T, which would result in a qualitatively different behaviour of the SdHO. From the measured m_c we find $v_F \approx 1.9$ and 2.2×10^6 m s^{-1} for the higher and lower $|n|$ in Fig. 2a, respectively. We have carried out measurements of m_c as in Fig. 2a for many different n, and the extracted values are presented in Fig. 2b for one of the devices. For the linear spectrum, m_c is expected to increase linearly with $k_F = (\pi n)^{1/2}$. In contrast, the experiment shows a superlinear

behaviour. Trying to fit the curves in Fig. 2b with the linear dependence $m_c(k_F)$, we find $v_F \geq 2.5 \times 10^6$ m s^{-1} at $n < 10^{10}$ cm^{-2} and $\leq 1.5 \times 10^6$ m s^{-1} for $n > 2 \times 10^{11}$ cm^{-2}, as indicated by the dashed lines. The observed superlinear dependence of m_c can be translated into v_F varying with n. Figure 2c replots the data in Fig. 2b in terms of $v_F = \hbar(\pi n)^{1/2}/m_c$, which shows a diverging-like behaviour of v_F near the neutrality point. This sharp increase in v_F (by nearly a factor of three with respect to v_F^*) contradicts to the linear model of graphene's spectrum but is consistent with the spectrum reshaped by e–e interactions (Fig. 1).

The data for m_c measured in four devices extensively studied in this work are collected in Fig. 3 and plotted on a logarithmic scale for both electrons and holes (no electron–hole asymmetry was noticed). The plot covers the experimental range of $|n|$ from 10^9 to nearly 10^{12} cm^{-2}. All the data fall within the range marked by the two dashed curves that correspond to constant $v_F = v_F^*$ and $v_F = 3 \times 10^6$ m s^{-1}. We can see a gradual increase in v_F as n increases, although the logarithmic scale makes the observed threefold increase less dramatic than in the linear presentation of Fig. 2c. Note that, even for the highest n in Fig. 3, the measured m_c do not reach the values expected for $v_F = v_F^*$ and are better described by $v_F \approx 1.3 v_F^*$. This could be due to the fact that the highest n values we could achieve for suspended graphene were still within a sub-10^{12} cm^{-2} range, in which some enhancement in v_F was reported for graphene on SiO$_2$ (refs 14,15). Alternatively, the difference could be due to the absence of a substrate in our case. To find out which of the effects dominates, we have studied high-μ devices made from graphene deposited on boron nitride[20,21] (its dielectric constant ε is close to that of SiO$_2$) and found that m_c in the range of n between ≈ 0.1 and 1×10^{12} cm^{-2} is well described by $v_F \approx v_F^*$ (Supplementary Information). This indicates that the observed difference in m_c at high n in Fig. 3 with respect to the values expected for v_F^* is likely to be due to the absence of dielectric screening in suspended graphene, which maximizes the interaction effects.

To explain the observed changes in v_F, let us first note that, in principle, not only e–e interactions but also other mechanisms such as electron–phonon coupling and disorder can lead to changes in v_F. However, the fact that the increase in v_F is observed over such a wide range of E rules out electron–phonon mechanisms, whereas
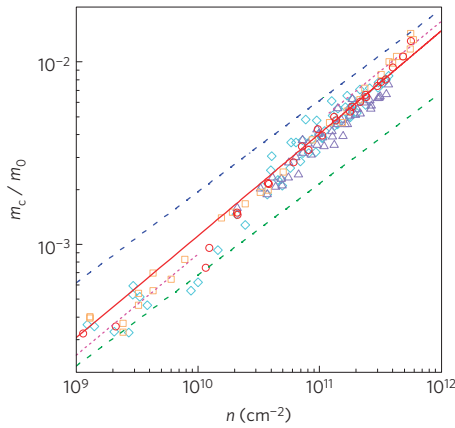
Figure 3 | Interaction-induced changes in the cyclotron mass. Different symbols are the measurements for different devices. The random scatter characterizes the statistical uncertainty for different samples and experiments. Blue and green dashed lines are the behaviour expected for the linear spectrum with constant v_F equal to v_F^* and 3×10^6 m s^{-1}, respectively. The solid red curve is for the spectrum renormalized by e–e interactions and described by equation (2) that takes into account the intrinsic screening self-consistently. The two dotted curves show that the interaction effects can also be described by a simpler theory (equation (1)) with an extra fitting parameter $\varepsilon_G(n)$, graphene's intrinsic dielectric constant. The best-fit curves yield $\varepsilon_G \approx 2.2$ and 4.9 at low and high ends of the n range.

the virtual absence of disorder in our suspended graphene makes the influence of impurities also unlikely. Therefore, we focus on e–e interactions, in which case graphene's spectrum is modified as shown in Fig. 1 and, in the first approximation, can be described by two related equations[8–10],

$$\frac{k}{v_F} \frac{\partial v_F}{\partial k} = -\frac{e^2}{4\varepsilon \hbar v_F} \qquad (1)$$

$$\frac{k}{v_F} \frac{\partial v_F}{\partial k} = -\frac{2}{\pi^2} \left[1 - \frac{4\hbar v_F \varepsilon}{N_f e^2} + \frac{8\hbar v_F \arccos\left(\frac{\pi N_f e^2}{8\hbar v_F \varepsilon}\right)}{N_f e^2 \pi \sqrt{1 - \left(\frac{\pi N_f e^2}{8\hbar v_F \varepsilon}\right)^2}} \right] \qquad (2)$$

where $\varepsilon = (1 + \varepsilon_s)/2$ describes the effect of a substrate with a dielectric constant ε_s. Equation (1) can be considered as the leading term in the renormalization group theory expansion in powers of $\alpha = e^2/\varepsilon \hbar v_F$, whereas (2) corresponds to a similar expansion in powers of $1/N_f$ (refs 8–10). The diagrams that depict these approximations are given in Supplementary Information. Importantly, equation (2) includes self-consistently the screening by graphene's charge carriers. An approximate scheme to incorporate this intrinsic screening while keeping the simplicity of equation (1) is to define an effective screening constant $\varepsilon_G(n)$ for the graphene layer and add it to ε (for suspended graphene $\varepsilon = \varepsilon_G$). Then, integrating equation (1), we obtain the logarithmic dependence[8]

$$v_F(n) = v_F(n_0) \left[1 + \frac{\alpha}{8\varepsilon_G} \ln(n_0/n) \right] \qquad (3)$$

where n_0 is the concentration that corresponds to the ultraviolet cutoff energy Λ, and $v_F(n_0)$ is the Fermi velocity near the cutoff. We assume $v_F(n_0) \equiv v_F^0$, its accepted value in graphene structures with weak e–e interaction.

Both approximations result in a similar behaviour of $v_F(n)$ and provide good agreement with the experiment. However,

equation (2) is more general and essentially requires no fitting parameters because Λ is expected to be of the order of graphene's bandwidth and affects the fit only weakly, as log (Λ). Alternatively, Λ can be estimated from the known value of v_F^0 at high $n \approx 5 \times 10^{12}$ cm^{-2} as $\Lambda = 2.5 \pm 1.5$ eV (ref. 22). The solid curves in Figs 2b,c and 3 show $m_c(n)$ and $v_F(n)$ calculated by integrating equation (2) and using $\Lambda \approx 3$ eV. The dependence captures all the main features of the experimental data. As for equations (1) and (3), they enable a reasonable fit by using $\varepsilon_G \sim 3.5$ over the whole range of our n. More detailed analysis (dotted curves in Fig. 3) yields $\varepsilon_G \approx 2.2$ and 5 for $n \sim 10^9$ and 10^{12} cm^{-2}, respectively. These values are close to those calculated in the random phase approximation, which predicts $\varepsilon_G = 1 + \pi N_f e^2/8\hbar v_F$. Using this expression in combination with equation (3) leads to a fit that is practically indistinguishable from the solid curve given by equation (2). This could be expected because equation (2) includes the screening self-consistently, also within the random phase approximation. The value of ε_G has recently become a subject of considerable debate[23–27]. Our data clearly show no anomalous screening, contrary to the recent report[27] that suggested $\varepsilon_G \approx 15$, but in good agreement with measurements reported in ref. 28.

Finally, a large number of theories have been predicting that the diverging contribution of e–e interactions at low E may result in new electronic phases[28–31], especially in the least-screened case of suspended graphene with $\varepsilon = 1$. Our experiments shows the diverging behaviour of v_F but no new phases emerge, at least for $n > 10^9$ cm^{-2} ($E > 4$ meV). Moreover, we can also conclude that there are no insulating phases even at E as low as 0.1 meV. To this end, we refer to Supplementary Information, in which we present the data for graphene's resistivity $\rho(n)$ in zero B. The peak at the neutrality point continues to grow monotonically down to 2 K, and $\rho(T)$ exhibits no sign of diverging (the regime of smearing by spatial inhomogeneity is not reached even at this T). This shows that, in neutral graphene in zero B, there is no gap larger than ≈ 0.1 meV. This observation is consistent with the fact that v_F increases near the neutrality point, which leads to smaller and smaller $\alpha = e^2/\hbar v_F$ at low E and, consequently, prevents the emergence of the predicted many-body gapped states.

References

1. Shankar, R. Renormalization-group approach to interacting fermions. *Rev. Mod. Phys.* **66,** 129–192 (1994).
2. Kotov, V. N., Pereira, V. M., Castro Neto, A. H. & Guinea, F. Electron–electron interactions in graphene: Current status and perspectives. Preprint at http://arxiv.org/abs/1012.3484 (2010).
3. Khveshchenko, D. V. Ghost excitonic insulator transition in layered graphite. *Phys. Rev. Lett.* **87,** 246802 (2001).
4. Gorbar, E. V., Gusynin, V. P., Miransky, V. A. & Shovkovy, I. A. Magnetic field driven metal-insulator phase transition in planar systems. *Phys. Rev. B* **66,** 045108 (2002).
5. Drut, J. E. & Lahde, T. A. Is graphene in vacuum an insulator? *Phys. Rev. Lett.* **102,** 026802 (2009).
6. Liang, W. J. *et al.* Fabry–Perot interference in a nanotube electron waveguide. *Nature* **411,** 665–669 (2001).
7. Abrikosov, A. A. & Beneslavskii, D. Possible existence of substances intermediate between metals and dielectrics. *Sov. Phys. JETP* **32,** 699–703 (1971).
8. Gonzalez, J., Guinea, F. & Vozmediano, M. A. H. Non-Fermi liquid behavior of electrons in the half-filled honeycomb lattice (a renormalization group approach). *Nucl. Phys. B* **424,** 595–618 (1994).
9. Gonzalez, J., Guinea, F. & Vozmediano, M. A. H. Marginal-Fermi-liquid behavior from two-dimensional Coulomb interaction. *Phys. Rev. B* **59,** 2474–2477 (1999).
10. Foster, M. S. & Aleiner, I. L. Graphene via large N: A renormalization group study. *Phys. Rev. B* **77,** 195413 (2008).
11. Novoselov, K. S. *et al.* Two-dimensional gas of massless Dirac fermions in graphene. *Nature* **438,** 197–200 (2005).

12. Zhang, Y. B., Tan, Y. W., Stormer, H. L. & Kim, P. Experimental observation of the quantum Hall effect and Berry's phase in graphene. *Nature* **438,** 201–204 (2005).
13. Kane, C. L. & Mele, E. J. Electron interactions and scaling relations for optical excitations in carbon nanotubes. *Phys. Rev. Lett.* **93,** 197402 (2004).
14. Li, Z. Q. *et al.* Dirac charge dynamics in graphene by infrared spectroscopy. *Nature Phys.* **4,** 532–535 (2008).
15. Luican, A., Li, G. & Andrei, E. Y. Quantized Landau level spectrum and its density dependence. *Phys. Rev. B* **83,** 041405 (2011).
16. Du, X., Skachko, I., Barker, A. & Andrei, E. Y. Approaching ballistic transport in suspended graphene. *Nature Nanotech.* **3,** 491–495 (2008).
17. Bolotin, K. I. *et al.* Ultrahigh electron mobility in suspended graphene. *Solid State Commun.* **146,** 351–355 (2008).
18. Castro, E. V. *et al.* Limits on charge carrier mobility in suspended graphene due to flexural phonons. *Phys. Rev. Lett.* **105,** 266601 (2010).
19. Sharapov, S. G., Gusynin, V. P. & Beck, H. Magnetic oscillations in planar systems with the Dirac-like spectrum of quasiparticle excitations. *Phys. Rev. B* **69,** 075104 (2004).
20. Dean, C. R. *et al.* Boron nitride substrates for high-quality graphene electronics. *Nature Nanotech.* **5,** 722–726 (2010).
21. Abanin, D. A. *et al.* Giant nonlocality near the Dirac point in graphene. *Science* **332,** 328–330 (2011).
22. de Juan, F., Grushin, A. G. & Vozmediano, M. A. H. Renormalization of Coulomb interaction in graphene: Determining observable quantities. *Phys. Rev. B* **82,** 125409 (2010).
23. Barlas, Y. *et al.* Chirality and correlations in graphene. *Phys. Rev. Lett.* **98,** 236601 (2007).
24. Hwang, E. H., Hu, B. Y. K. & Sarma, S. Density dependent exchange contribution to compressibility in graphene. *Phys. Rev. Lett.* **99,** 226801 (2007).
25. Sheehy, D. E. & Schmalian, J. Quantum critical scaling in graphene. *Phys. Rev. Lett.* **99,** 226803 (2007).
26. Kotov, V. N., Uchoa, B. & Neto, A. H. C. Electron–electron interactions in the vacuum polarization of graphene. *Phys. Rev. B* **78,** 035119 (2008).
27. Reed, J. P. *et al.* The effective fine-structure constant of freestanding graphene measured in graphite. *Science* **330,** 805–808 (2010).
28. Bostwick, A. *et al.* Observation of plasmarons in quasi-free-standing doped graphene. *Science* **328,** 999–1002 (2010).
29. Khveshchenko, D. V. Ghost excitonic insulator transition in layered graphite. *Phys. Rev. Lett.* **87,** 246802 (2001).
30. Gorbar, E. V., Gusynin, V. P., Miransky, V. A. & Shovkovy, I. A. Magnetic field driven metal–insulator phase transition in planar systems. *Phys. Rev. B* **66,** 045108 (2002).
31. Drut, J. E. & Lähde, T. A. Is graphene in vacuum an insulator? *Phys. Rev. Lett.* **102,** 026802 (2009).

Additional information

The authors declare no competing financial interests. Supplementary information accompanies this paper on www.nature.com/naturephysics. Reprints and permissions information is available online at http://www.nature.com/reprints. Correspondence and requests for materials should be addressed to F.G.

Dirac cones reshaped by interaction effects in suspended graphene

D. C. Elias *et al*

#1. Experimental devices

Graphene monolayers were obtained by micromechanical cleavage of graphite on top of an oxidized Si wafer [S1]. In this work, we specially selected long and narrow crystals (typically, 2 to 4 μm wide) which allowed us to avoid dry etching of graphene mesas. Two-terminal devices such as shown in Fig. 2 of the main text were then designed and fabricated by using standard lithography and deposition techniques. The 300 nm SiO₂ layer was partially etched in a buffered HF solution to leave graphene hanging above the substrate. The metal leads (5 nm Cr followed by 100 nm of Au) remained not fully etched underneath and served as a mechanical support. These fabrication procedures are similar to those described in refs. [S2-S5].

The current annealing was performed in situ, in a liquid-helium bath by applying voltage between adjacent contacts. Current densities of ~1 mA/μm were necessary to heat suspended graphene locally to $T > 600^{\circ}C$ [S5]. Our devices either fail or anneal after a minor (<1%) increase in applied voltage, which we believe is an indication that the real T of annealing could be even higher than suggested in ref. [S5].
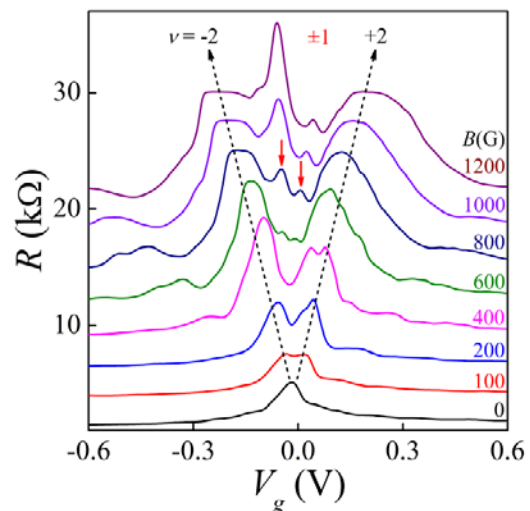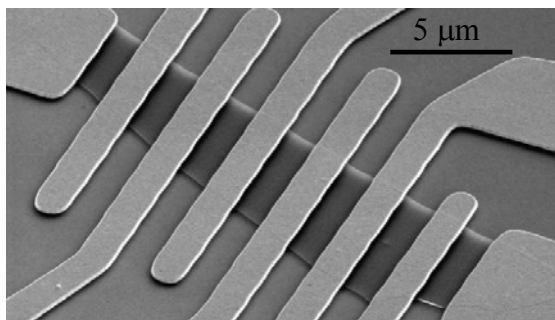

Figure S1. Our graphene devices. Left – Scanning electron micrograph of another suspended device, different from the one shown in Fig. 2a. Right – Typical behaviour of $R(V_g)$ measured at 2K. The curves are shifted for clarity. The QHE in the two probe geometry is known to lead to plateaux in R at $h/\nu e^2$. Such QHE plateaux are clearly seen in our devices below 0.1T. The dominant QHE plateau (filling factor $\nu = \pm 2$) at $R \approx 12.8k\Omega$ is first formed at negative gate voltages where μ is somewhat higher. Additional peaks at lower $|V_g|$ correspond to $\nu = \pm 1$ and indicate either spin or valley splitting.

Figure S1 shows two-terminal resistance R as a function of gate voltage V_g in different magnetic fields B. We refer to our measurements as two-terminal because the supporting metal contacts overlap with the current path (Fig. S1), that is, they are invasive [S6,S7]. In this measurement geometry, we found little difference whether we used two- or four-probe measurement geometry because of the relatively small resistance of the metal leads.

As one can see in Figure S1, the Landau level splitting occurs at $B \sim 100$ G (red and blue curves). The observation of SdHO requires $\mu B \approx 1$, which allows us to estimate quantum mobility μ as $\sim 10^6$ cm^2/Vs [S3,S4,S8]. This value is in good agreement with the field-effect μ found from changes in conductivity σ as a function of n in zero B [S4] (also, see Fig. S2). As a further indication of the graphene quality, one can see that the first quantum Hall effect (QHE) plateau develops at 600 G for holes (green curve; negative V_g) and becomes fully formed for both electrons and holes at 1000 G (violet). Also, the 4-fold degeneracy of the lowest LL becomes lifted already at ~ 600 G (green).
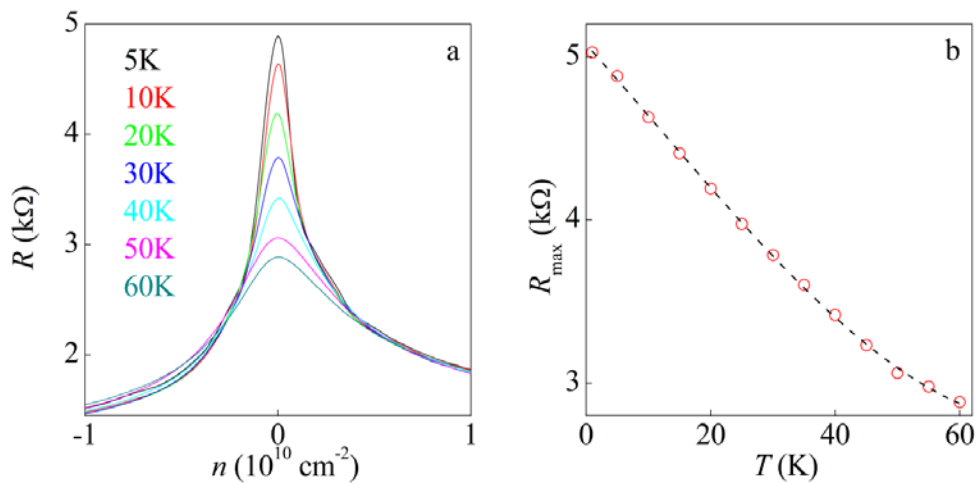

Figure S2. No discernable gap in neutral graphene. (**a**) – R as a function of concentration n in a suspended device at various T in zero B. The peak at the Dirac point continues to sharpen with decreasing T but R remains finite, with no sign of a gap: that is, $R(T)$ does not diverge at $T \rightarrow 0$. (**b**) – The device's maximum resistance as function of T. The points are the experimental data and the dashed curve is a guide to the eye. The practically linear dependence $R(T)$ is puzzling and may be related to the transition from the dependence $R \propto 1/T^2$ found at high T (due to thermally generated carriers at the NP) to the pseudo-diffusive regime with a finite conductivity in the limit of low T.

Charge inhomogeneity δn is usually estimated from smearing of the resistance peak near the NP. However, in our devices, the peak continues sharpening down to 2 K (Fig. S2), the lowest T in the current experiments. This shows that the thermal generation of electrons and holes at the NP

dominates any remnant charge inhomogeneity, which yields δn less than $\sim 10^8$ cm^{-2}, that is of about one electron per square μm. In order to extract cyclotron mass m_c it was necessary to measure SdHO at many different T. This effectively led to δn being determined by T rather than real inhomogeneity and limited our m_c measurements to $n \geq 10^9$ cm^{-2}. Furthermore, the smooth monotonic behaviour of R as a function of both n and T (see Fig. S2) implies that, except for the discussed logarithmic corrections, no dramatic reconstruction of the Dirac spectrum occurs at E down to 1 meV ($n \approx 10^8$ cm^{-2}). Otherwise, one would expect to observe some anomalies in $R(n,T)$ whereas the presence of an energy gap larger than ~ 0.1 meV would be seen as diverging $R(T \rightarrow 0)$.

#2. Analysis of Shubnikov–de Haas oscillations

We have measured the cyclotron mass m_c in graphene by analysing T dependence of SdHO. This well-established approach has widely been used in literature [S9-S10]. In the case of graphene, the approach provided accurate measurements of m_c which retrospectively were found in good agreement with the results obtained by other techniques (e.g., magneto-optics and tunnelling microscopy). In brief, our procedures involved measurements of suspended graphene's conductance $G = 1/R$ as a function of n at a given B. Then, we changed T and repeated the measurements. T and B were always chosen to keep far away from the QHE regime so that changes in conductance $\Delta G << G$.
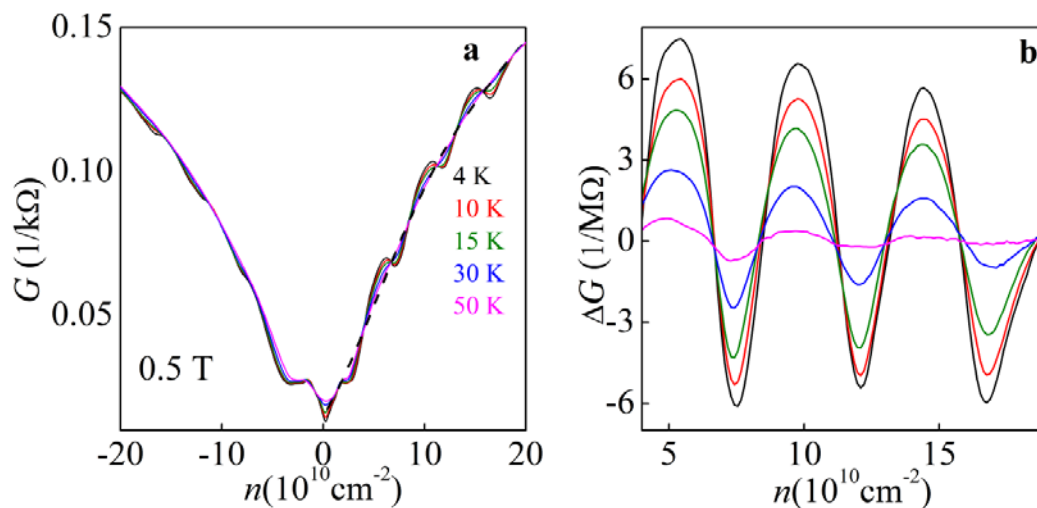

Figure S3. (a) – $G(n)$ for a suspended graphene device in $B = 0.5$ T at several T. The dashed curve indicates the smooth polynomial background. (b) – Curves from (a) after the subtracting the background.

Examples of our raw data are shown Figure S3a. SdHO are clearly seen on top of the standard V-shaped background. This background is smooth and, for easier analysis, can be subtracted. We have done this separately for electrons and holes. To standardise the procedures, we normally defined the

background by fitting a 4th-order polynomial to one of high-T curves $G(n)$ with no discernable oscillations, as illustrated in Fig. S3a. The subtraction resulted in curves such as shown in Fig. S3b. The SdHO amplitude was then calculated as the difference between ΔG in maxima and minima. This yielded the data such as shown in Fig. 2a of the main text. Typically, we used 10 different T to obtain each value of m_c. The results were practically independent of the choice of subtracted background and other procedural details, essentially due to the fact that we analyzed the difference between minima and maxima.

#3. Influence of a dielectric substrate

As found in many experiments, graphene on SiO_2 exhibits the Fermi velocity $v^*_F \approx 1.05 \pm 0.1 \times 10^6$ m/s for the typically accessible range of $n \sim 10^{12}$ cm^{-2}. The measurements for suspended graphene reported in the main text show a slightly higher v_F (15 to 25%) for the same range of n. This disagreement can be attributed to the absence of dielectric screening in the suspended devices. To prove this and exclude any systematic error arising due to the use of devices with drastically different mobilities (μ differ by a factor of 100 for suspended graphene and graphene on SiO_2), we performed measurements of $m_c(n)$ for graphene on boron nitride (GBN). The latter devices allow $\mu > 100,000$ cm^2/V and, at the same time, e-e interactions are screened in a manner similar to the case of graphene on SiO_2 (boron nitrite exhibits $\varepsilon_s \approx 5$ [S11]).

Our GBN devices were fabricated as described in refs. [S12,S13] and one of the studied devices is shown in Fig. S4. To find m_c, we performed the same measurements and analysis as described in the previous chapter. The resulting dependence $m_c(n)$ is shown in Fig. S4. The accessible range of n was limited to $\geq 10^{11}$ cm^{-2} due to charge inhomogeneity that was smaller than in graphene on SiO_2 but still significant, in agreement with refs. [S13,S14]. The dashed curve corresponds to a constant $v_F = v^*_F$ and provides an excellent description of our data within this limited range of n, similar to the case of graphene on SiO_2. This strongly supports the argument that v_F in graphene on a substrate is lower than in suspended graphene due to dielectric screening in the former case.

To check our analysis of the renormalized spectrum for consistency, the solid and dotted curves in Figure S4 show $m_c(n)$ calculated by using to equation (2). The dotted line is the same theory curve shown in Figs. 2c and 3 of the main text for suspended graphene, which corresponds to the case of $\varepsilon = 1$ and $\Lambda \approx 3$eV. On the other hand, the solid line was calculated by using the same equation and only adding the dielectric screening due to boron nitride with no change in other parameters. The agreement between the experiment and theory is impressive and shows that our theoretical

description is able to explain not only the *n* dependence of the Fermi velocity but, also, its dependence on dielectric screening.
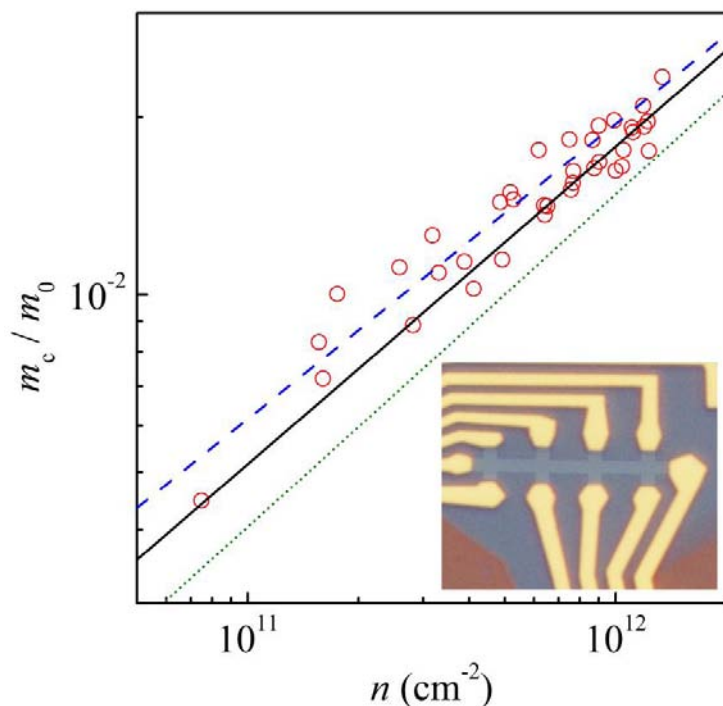

Figure S4. Cyclotron mass as function of *n* for graphene on boron nitride. The symbols are experimental data; the dashed line is the non-interacting behaviour with constant $v_F = v^*_F$. The RGT approach, which is used in the main text to describe $m_c(n)$ in suspended graphene over a wide range of *n*, is also consistent with the limited-range data for GBN devices. The dotted curve is given by equation (2) of the main text ($\varepsilon=1$; $\Lambda =3$eV) whereas the solid one is for $\varepsilon_s=5$; $\Lambda =3$eV (no fitting parameters). The inset shows an optical micrograph of a Hall bar device made from graphene deposited on BN (no encapsulating top layer [S13]). For clarity, the contrast of the 1μm wide graphene mesa was digitally enhanced.

#4. Interaction renormalization of the Dirac spectrum in various approximations

Near the NP, screening is weak due to the low density of states and completely suppressed in neutral graphene because the density of states goes to zero. As a result, electronic levels become increasing affected by e-e interactions as their energy approaches the Dirac point. The Hartree-Fock correction to the quasiparticle energy is given by

$$\delta E \approx \pm \int d^2 \vec{k}' \frac{2\pi e^2}{\varepsilon |\vec{k}-\vec{k}'|} \left(\frac{1}{2} \pm \frac{\vec{k} \cdot \vec{k}'}{|\vec{k}||\vec{k}'|} \right) \approx \pm \frac{e^2}{4\varepsilon} \ln\left(\frac{k_\Lambda}{|\vec{k}|} \right)$$ (S1)

where k_Λ is the upper limit in the momentum integral, and the signs ± correspond to electrons and holes, respectively. This equation yields a change in the Fermi velocity δv_F which becomes a function of momentum $\vec{k}$

$$\delta v_F \approx \frac{e^2}{4\varepsilon} \ln\left(\frac{k_\Lambda}{|\vec{k}|} \right)$$ (S2).
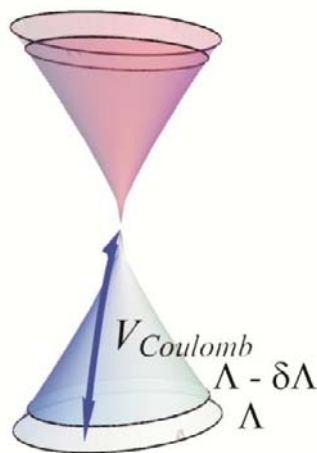
Figure S5. Sketch for the Renormalization Group procedure used to explain the experimental observations. Coulomb interactions between low- and high- E states deplete the electronic spectrum near the Dirac point.

An improvement over the Hartree-Fock approximation can be achieved by calculating changes in v_F for low-E quasiparticles, which are induced by their interaction with high-E excitations in the interval of energies $\Lambda - \delta\Lambda \leq E \leq \Lambda$ and defining a new model for the electronic spectrum in which these excitations are removed, as schematically shown in Fig. S5. Within this model, v_F is described by

$$\hbar v_F(\Lambda - \delta\Lambda) \approx \hbar v_F(\Lambda) + \frac{e^2}{4\varepsilon}\frac{\delta\Lambda}{\Lambda} \tag{S3}$$

Or, alternatively

$$\hbar k \frac{\partial v_F}{\partial k} = -\frac{e^2}{4\varepsilon} \tag{S4}.$$

This result reproduces equation (1) in the main text. Using the same analysis, it can be shown that there is no need to modify other parameters in the Hamiltonian. This scheme defines the RGT transformation that is exact in the limit $\alpha = e^2/\hbar v_F \ll 1$. The self energy diagram that gives rise to eq. (1) is shown in Fig. S6a. However, the above limit is not valid for graphene where the effective fine structure constant $\alpha \approx 2$. The fact that α is of order unity makes it problematic to use the standard expansion methods. This problem can be overcome by using the expansion in powers of $1/N_f$ as described below.
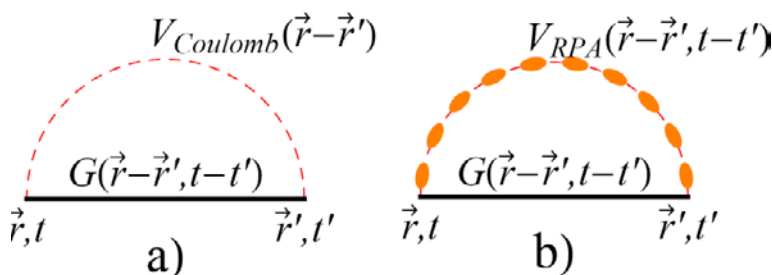

Figure S6. (a) – Diagram that leads to eq. (1) of the main text. (b) – The diagram takes into account self-screening.

Equations (1) and (S1-S4) include only screening effects due to environment of the graphene sheet, which is described by the dielectric constant ε. The intrinsic screening by charge carriers can also be added in a phenomenological way by redefining ε and introducing ε_G as discussed in the main text. Alternatively, a better description can be achieved by self-consistently including the screening

processes into the interaction line in Fig. S6a. The resulting diagram is shown in Fig. S6b, and this leads to equation (2) of the main text. Furthermore, it can be shown that the infinite summation of polarization bubbles in the second diagram results in the approximation that becomes exact if $N_f \gg 1$. In graphene, $N_f = 4$ so that the approximation's accuracy is comparable to similar calculations used in quantum chromodynamics [S15].

The analysis of experimental results in the main text is mainly based on the above eq. (2) because this approach does not require any prior knowledge of the electronic polarizability, α or ε_G. Furthermore, eq. (2) allows us to determine the value of ε_G for different n, which has become a subject of debate after anomalously large $\varepsilon_G \approx 15$ were reported [S16]. We have found significantly smaller ε_G (see the main text). This is in agreement with the RGT expectations and, also, the measurements of electron-plasmon satellites ("plasmarons"), which were reported in ref. [S17] and yielded the bare fine structure constant $\alpha \approx 2.2$ (cf. the best fits to our data gives $\alpha \approx 2.4$).

Finally, it is instructive to compare the renormalized Dirac spectrum inferred from our measurements and shown in Fig. 1 with the excitation spectra modified by interactions and schematically shown in Fig. 1H of ref. [S17]. In our case, we probe v_F as function of n (or the Fermi energy E_F) and its value changes each time we change the low energy cut-off, that is, E_F. The spectrum under the Fermi surface is expected to be linear but its slope (that is, v_F) changes from measurement to measurement. In ref. [S17], the excitation spectra for Dirac fermions are probed underneath the Fermi surface and the cut-off is fixed for all E by either a given n or excitations' energy, whichever value is larger. There is no disagreement between the two figures: these are just the spectra referring to different many-body phenomena.

#5. Influence of disorder

The RGT flow that describes the dependence of v_F on energy leads to changes in this parameter, which can be comparable to v^0_F, the initial values of the parameter itself. On the other hand, other couplings such as electron-phonon [S18] and electron-plasmon interactions [S17] can be treated within a perturbation theory because they do not lead to logarithmic divergences. Therefore, it can be expected that their effect on the Fermi velocity does not exceed a fraction of its value and, accordingly, they cannot explain the large enhancement observed in the experiment. The only other interaction that can lead to logarithmic renormalization is the coupling to some types of scalar and gauge random disorder [S19-S21]. However, the arising corrections have the opposite sign with

respect to that due to electron-electron interactions. Furthermore, the disorder can be described by the dimensionless parameter

$$\Delta \sim \langle V^2 \rangle (l/v_F)^2 \qquad\qquad (S5)$$

where $\langle V^2 \rangle$ gives the average value of the disorder, and l is the range over which it is correlated. This gives rise to a scattering time τ

$$h/\tau \sim \Delta \times E_F \qquad\qquad (S6)$$

where E_F is the Fermi energy. In order to significantly change the effect of electron-electron interaction, the value of Δ should be comparable to $e^2/\hbar v_F$. The long mean free path, characteristic of the suspended graphene studied in this work, rule out the existence of such strong disorder.

Supplementary References

[S1]   K. S. Novoselov *et al*. *PNAS* **102**, 10451 (2005).

[S2]   X. Du *et al*. *Nature Nanotech*. **3** 491 (2008).

[S3]   K. I. Bolotin *et al*. *Solid State Commun*. **146** 351 (2008).

[S4]   E. V. Castro et al. *Phys. Rev. Lett*. **105**, 266601 (2010).

[S5]   K. I. Bolotin et al. *Nature* **462** 351 (2008).

[S6]   P. Blake *et al*. *Solid State Commun* **149**, 1068 (2009)

[S7]   J. R. Williams *et al*. *Phys. Rev. B*. **80**, 045408 (2009)

[S8]   M. Monteverde *et al*. *Phys. Rev. Lett*. **104**, 126801 (2010).

[S9]   J. L. Smith and P. J. Stiles, Phys. Rev. Lett. 29, 102–104 (1972)

[S10]   W. Pan and D. C. Tsui, Phys. Rev. B 59, 10208–10211 (1999)

[S11]   R. V. Gorbachev *et al*. *Small* **7**, 465 (2011).

[S12]   C. R. Dean *et al*. *Nature Nanotech*. **5**, 722 (2010).

[S13]   A. S. Mayorov *et al*. *Nano Lett*. to appear (2011) (see arXiv:1103.4510).

[S14]   J. Xue *et al*. *Nature Mater*. **10**, 282 (2011)

[S15]   S. Coleman, *Aspects of Symmetry*, Cambridge University Press (1985).

[S16]   J. P. Reed et al. *Science* **330**, 805 (2010).

[S17]   A. Bostwick et al. *Science* **328**, 999 (2010).

[S18]   C.-H. Park et al. *Phys. Rev. Lett*. **99**, 086804 (2007).

[S19]   T. Stauber et al. *Phys. Rev. B* 71, 041406, (2005).

[S20]   M. S. Foster and I. L. Aleiner, *Phys. Rev. B*, **77**, 195413 (2008).

[S21]   I. F. Herbut et al. *Phys. Rev. Lett*. **100**, 046403 (2008).